Improving Quality of Medical Image Compression Using Biorthogonal CDF Wavelet Based on Lifting Scheme and SPIHT Coding

Mohammed Beladgham[1,2], Abdelhafid Bessaid[2], Abdelmounaim Moulay Lakhdar[1], Abdelmalik Taleb-Ahmed[3]

Abstract: As the coming era is that of digitized medical information, an important challenge to deal with is the storage and transmission requirement**s** of enormous data, including medical images. Compression is one of the indispensable techniques to solve this problem. In this work, we propose an algorithm for medical image compression based on a biorthogonal wavelet transform CDF 9/7 coupled with SPIHT coding algorithm, of which we applied the lifting structure to improve the drawbacks of wavelet transform. In order to enhance the compression by our algorithm, we have compared the results obtained with wavelet based filters bank. Experimental results show that the proposed algorithm is superior to traditional methods in both lossy and lossless compression for all tested images. Our algorithm provides very important PSNR and MSSIM values for MRI images.

Keywords: Medical image, Compression, Biorthgonal wavelets, CDF9/7, Lifting scheme, SPIHT.

1 Introduction

The massive use of numerical methods in medical imaging (MRI, X scanner, nuclear medicine, etc.) today generates increasingly important volumes of data. The problem becomes even more critical with the generalisation of 3D sequence. So it is necessary to use compressed images in order to limit the amount of data to be stored and transmitted.

Many compression schemes by transformation have been proposed, we can cite the standards JPEG images, MPEG 1 and 2 for video compression. All of these standards are based on the discrete cosine transform (DCT) [1].

Over the past ten years, the wavelets (DWT) have had a huge success in the field of image processing, and have been used to solve many problems such as

---

[1]Departement of Electronic, Bechar University, Bechar 08000, Algeria. E-mail: beladgham.tlm@gmail.com
[2]Genie-Biomedical Laboratory, Departement of Electronic, Abou bekr Belkaid University, Tlemcen 13000, Algeria.
[3]Biomecanic Laboratory, Valencienne University, France.

image compression and restoration [2]. However, despite the success of wavelets in various fields of image processing such as encoding, weaknesses have been noted in its use in the detection and representation of the objects' contours. The wavelets transform and other classical multi-resolutions decompositions seem to form a restricted and limited class of opportunities for multi-scale representations of multidimensional signals.

To overcome this problem, new multi resolution decompositions better adapted to the representation of images are used. This is the case of decomposition by lifting scheme.

In this work we propose the lifting structure algorithm for MRI image compression. For this reason, this paper is divided into three parts: the first is devoted to a representation of the Lifting scheme, then we present the biorthgonal wavelet CDF 9/7.

In order to enhance image compression by our algorithm, we compare the PSNR and MSSIM results obtained with the existing techniques namely the wavelets filter bank.

2   Wavelet Transforms

The wavelet transform (WT), in general, produces floating point coefficients. Although these coefficients are used to reconstruct an original image perfectly in theory, the use of finite precision arithmetic and quantization results in a lossy scheme.

Recently, reversible integer WT's (WT's that transform integers to integers and allow perfect reconstruction of the original signal) have been introduced [3, 4]. In [5], Calderbank et al. introduced how to use the lifting scheme presented in [6], where Sweldens showed that the convolution based biorthogonal WT can be implemented in a lifting-based scheme as shown in Fig. 1 for reducing the computational complexity. Note that only the decomposition part of WT is depicted in Fig. 1 because the reconstruction process is just the reverse version of the one in Fig. 1. The lifting-based WT consists of splitting, lifting, and scaling modules and the WT is treated as a prediction-error decomposition. It provides a complete spatial interpretation of WT. In Fig. 1, let X denote the input signal, and X_{L1} and X_{H1} be the decomposed output signals, where they are obtained through the following three modules of lifting-based 1DWT:

1. **Splitting:** In this module, the original signal X is divided into two disjoint parts, i.e., $X_e(n) = X(2n)$ and $X \ X_0(n) = X(2n+1)$ that denote all even-indexed and odd-indexed samples of X, respectively [7].

164

2. **Lifting:** In this module, the prediction operation P is used to estimate $X_0(n)$ from $X_e(n)$ and results in an error signal $d(n)$ which represents the detailed part of the original signal. Then we update $d(n)$ by applying it to the update operation U, and the resulting signal is combined with $X_e(n)$ to $s(n)$ estimate, which represents the smooth part of the original signal.

3. **Scaling:** A normalization factor is applied to $d(n)$ and $s(n)$, respectively. In the even-indexed part $s(n)$ is multiplied by a normalization factor K_e to produce the wavelet subband X_{L1}. Similarly in the odd-index part the error signal $d(n)$ is multiplied by K_0 to obtain the wavelet subband X_{H1}.
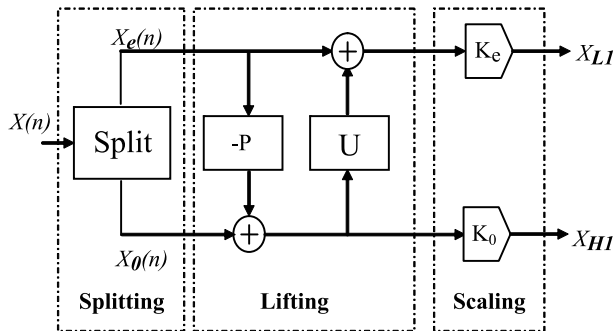

Fig. 1 – *The lifting-based* WT.

Note that the output results of X_{L1} and X_{H1} obtained by using the lifting-based WT are the same as those of using the convolution approach for the same input even if they have completely different functional structures. Compared with the traditional convolution-based WT, the lifting-based scheme has several advantages. First, it makes optimal use of similarities between the highpass and lowpass filters; the computation complexity can be reduced by a factor of two. Second, it allows a full in-place calculation of the wavelet transform. In other words, no auxiliary memory is needed.

3   Biorthogonal Wavelets CDF 9/7

This article deals with biorthogonal wavelet 9/7. These wavelets are part of the family of symmetric biorthogonal wavelet CDF. The low pass filters associated with wavelet 9/7 have $p = 9$ coefficients in the analysis, $p = 7$ coefficients to synthesize, as described in **Table 1**. The biorthogonal wavelets 9/7 are illustrated in Fig. 2, they have $N = 4$ null moments in analysis, and $\tilde{N} = 4$ in synthesis.

The wavelets 9/7 have a great number of null moments for a relatively short support. They are more symmetrical and very close to orthogonality. This is an important feature in coding which ensures that the reconstruction error is very close to the quantization error in terms of mean squared error. Antonini and Barlaud were the first [8] to show the superiority of the biorthogonal wavelet transform 9/7 for the decorrelation of natural images. It has been widely used in image coding [9, 10] and is used by the JPEG-2000 codec [11].

Table 1a

The analysis filter coefficients.

	Analysis filter coefficients	
i	Low-pass filter	High-pass filter
0	0.6029490182363579 0.6029490182363579	+ 1.115087052457000
±1	+ 0.266864118442875	+ 0.591271763114250
±2	− 0.078223266528990	− 0.057543526228500
±3	− 0.016864118442875	− 0.091271763114250
±4	+ 0.026748757410810	

Table 1b

The synthesis filter coefficients.

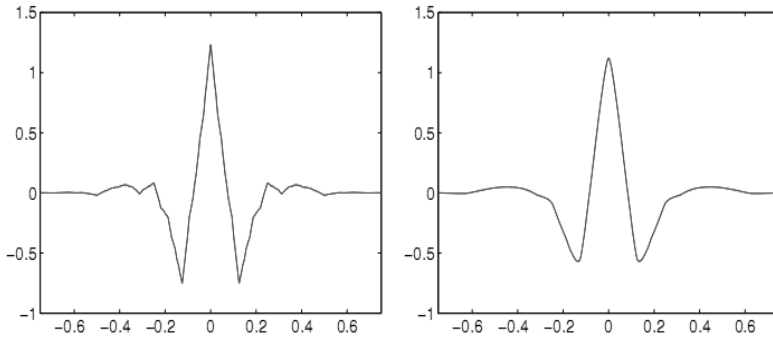|	Synthesis filter coefficients	
i	Low-pass filter	High-pass filter
0	+ 1.115087052457000	0.6029490182363579
±1	− 0.591271763114250	− 0.266864118442875
±2	− 0.057543526228500	− 0.078223266528990
±3	+ 0.091271763114250	+ 0.016864118442875
±4		+ 0.026748757410810

Fig. 2 – CDF 9/7 *wavelet* ψ *and* ψ̃ *dual.*

The Lifting scheme of the biorthogonal transform 9/7 goes through of four steps: two prediction operators and two update operators as shown it Fig. 3 [12, 13].
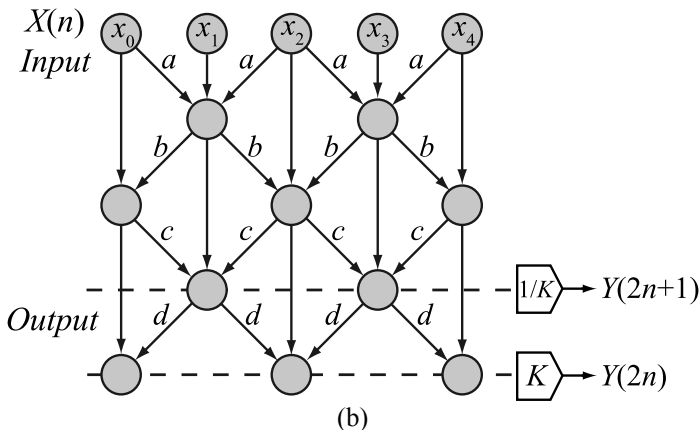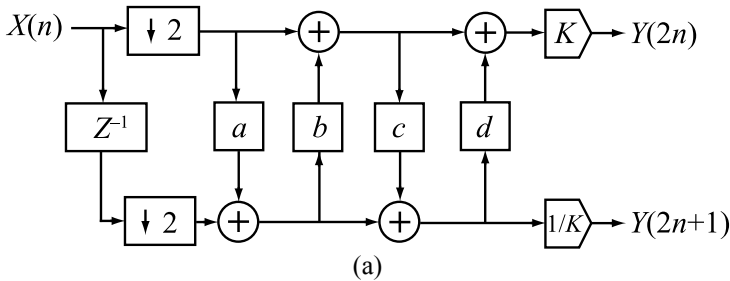

(a)

(b)

Fig. 3 – *Split, Predict and Update Steps of forward*
CDF 9/7 wavelet using Lifting scheme;
(a) *Lifting implementation of the analysis side of the* CDF 9/7 *filter bank;*
(b) *Structure of the* CDF 9/7 *filter.*

167

For lifting implementation, the CDF 9/7 wavelet filter pair can be factorized into a sequence of primal and dual lifting. The most efficient factorization of the polyphase matrix for the 9/7 filter is as follows [14, 15]:

$$P(Z) = \begin{bmatrix} 1 & a(1+Z^{-1}) \\ 0 & 1 \end{bmatrix} \cdot \begin{bmatrix} 1 & 0 \\ b(1+Z) & 1 \end{bmatrix} \cdot \begin{bmatrix} 1 & c(1+Z^{-1}) \\ 0 & 1 \end{bmatrix} \cdot$$
$$\cdot \begin{bmatrix} 1 & 0 \\ d(1+Z) & 1 \end{bmatrix} \cdot \begin{bmatrix} K & 0 \\ 0 & 1/K \end{bmatrix} \cdot \tag{1}$$

The following equation describes the four "lifting" steps and the two "Scaling" steps.

$$\begin{cases} Y(2n+1) & \leftarrow & X(2n+1)+(a \times [X(2n)+X(2n+2)]), \\ Y(2n) & \leftarrow & X(2n)+(b \times [Y(2n-1)+Y(2n+1)]), \\ Y(2n+1) & \leftarrow & Y(2n+1)+(c \times [Y(2n)+Y(2n+2)]), \\ Y(2n) & \leftarrow & Y(2n)+(d \times [Y(2n-1)+Y(2n+1)]), \end{cases} \tag{2}$$

$$\begin{cases} Y(2n+1) & \leftarrow & -K \times Y(2n+1), \\ Y(2n) & \leftarrow & (1/K) \times Y(2n), \end{cases} \tag{3}$$

where the values of the parameters are:

$$a = -1.586134342,$$
$$b = -0.0529801185,$$
$$c = 0.8829110762,$$
$$d = -0.4435068522,$$
$$K = 1.149604398.$$

The synthesis side of the filter bank simply inverts the scaling, and reverses the sequence of the lifting and update steps. Fig. 4 shows the synthesis side of the filter bank using lifting.
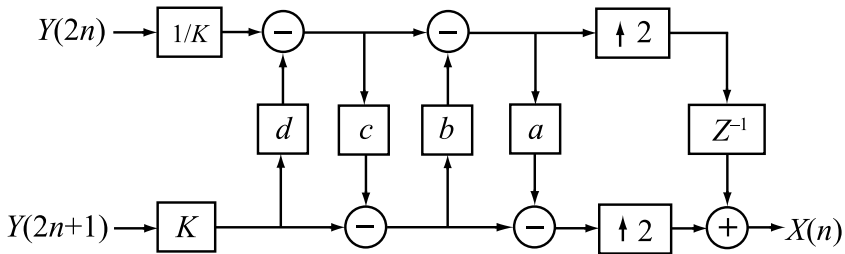

Fig. 4 – *Lifting implementation of the synthesis side of the* CDF 9/7 *filter bank.*

4 SPIHT Coding Scheme

When the decomposition image is obtained, we try to find a way to code the wavelet coefficients into an efficient result, taking redundancy and storage space into consideration. SPIHT [7] is one of the most advanced schemes available, even outperforming the state-of-the-art JPEG 2000 in some situations. The basic principle is the same; a progressive coding is applied, processing the image respectively to a lowering threshold. The difference is in the concept of zerotrees (spatial orientation trees in SPIHT). This is an idea that takes into consideration bounds between coefficients across subbands at different levels [9]. The first idea is always the same: if there is a coefficient at the highest level of the transform in a particular subband which considered insignificant against a particular threshold, it is very probable that its descendants in lower levels will be insignificant too. Therefore we can code quite a large group of coefficients with one symbol. Fig. 5 shows how a spatial orientation tree is defined in a pyramid constructed with recursive four subbands splitting. The coefficients are ordered hierarchically. According to this relationship, the SPIHT algorithm saves many bits that specify insignificant coefficients [16].
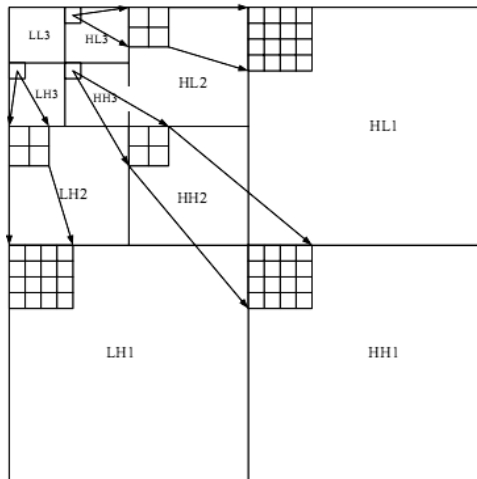

Fig. 5 – *Parent-child relationship.*

The flowchart of SPIHT is presented in Fig. 6. As a First step, the original image is decomposed into ten subbands. Then the method finds the maximum and the iteration number. Second, the method puts the DWT coefficients into a sorting pass that finds the significance coefficients in all coefficients and encodes the sign of these significance coefficients. Third, the significance coefficients that can be found in the sorting pass are put into the refinement pass that uses two bits to exact the reconstruct value for approaching to real value.

The first second and third steps are iterative, then iteration decreases the threshold ($T_n = T_{n-1}/2$) and the reconstructive value ($R_n = R_{n-1}/2$). As a fourth step, the encoding bits access entropy coding and then transmit [17]. The result is in the form of a bitstream.

All of the wavelet-based-image encoding algorithms improve the compression rate and the visual quality, but the wavelet-transform computation is a serious disadvantage of those algorithms.
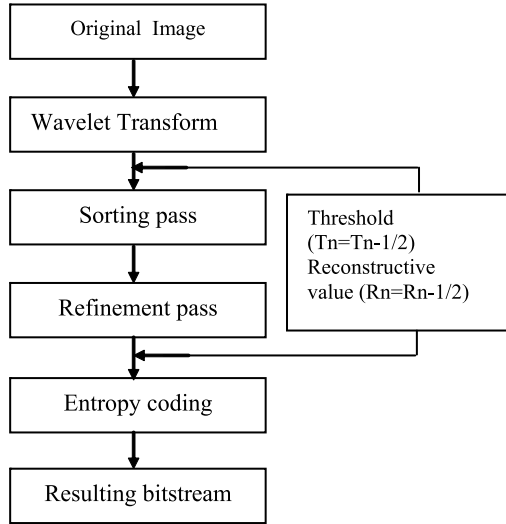

Fig. 6 – *Flowchart of* SPIHT.

5   Compression Quality Evaluation

The Peak Signal to Noise Ratio (PSNR) is the most commonly used as a measure of quality of reconstruction in image compression. The PSNR are identified using the following formulate:

$$PSNR = 10\log_{10}\left(\frac{(\text{Dynamics of image})^2}{MSE}\right). \qquad (4)$$

Mean Square Error (MSE) which requires two $M \times N$ grayscale images I and $\hat{I}$, where one of the images is considered as a compression of the other is defined as:

$$MSE^2 = \frac{1}{M \times N}\sum_{1=1}^{i=M}\sum_{j=1}^{j=N}\left(I(i,j) - \hat{I}(i,j)\right)^2. \qquad (5)$$

170

Usually an image is encoded on 8 bits. It is represented by 256 gray levels, which vary between 0 and 255, the extent of image dynamics is 255.

The structural similarity index (SSIM)

The PSNR measurement gives a numerical value on the damage, but it does not describe its type. Moreover, as is noted in [18, 19], it does not quite represent the quality perceived by human observers.

For medical imaging applications, where images are degraded must eventually be examined by experts, traditional evaluation remains insufficient. For this reason, objective approaches are needed to assess the medical imaging quality.

We then evaluate a new paradigm to estimate the quality of medical images, specifically the ones compressed by wavelet transform, based on the assumption that the human visual system (HVS) is highly adapted to extract structural information.

The similarity index compares the brightness, contrast and structure between each pair of vectors, where the structural similarity index (SSIM) between two signals x and y is given by the following expression [20, 21]:

$$\text{SSIM}(x, y) = l(x, y)c(x, y)s(x, y). \tag{6}$$

However, the comparison of brightness is determined by the following expression:

$$l(x, y) = \frac{2\mu_x\mu_y + C_1}{\mu_x + \mu_y + C_1}, \tag{7}$$

where the average intensity of signal x is given by: $\mu_x = \frac{1}{N}\sum_{i=1}^{N} x_i$, $C_1 = (K_1 L)^2$, the constant $K_1 \ll 1$, and L is the dynamic row of the pixel values (255 for an image in gray scale coded on 8 bits).

The function of contrast comparison takes the following form:

$$c(x, y) = \frac{2\sigma_x\sigma_y}{\sigma_x^2 + \sigma_y^2 + C_2}, \tag{8}$$

where $\sigma_x = \sqrt{\mu_x(x^2) - \mu_x^2}$ is the standard deviation of the original signal x, $C_2 = (K_2 L)^2$, and the constant $K_2 \ll 1$.

The function of structure comparison is defined as follows:

$$s(x, y) = \frac{\sigma_{xy} + C_3}{\sigma_x\sigma_y + C_3} = \frac{\text{cov}(x, y) + C_3}{\sigma_x\sigma_y + C_3}, \tag{9}$$

where $\mathrm{cov}(x,y) = \mu_{xy} - \mu_x \mu_y$, and $C_3 = \dfrac{C_2}{2}$.

Then the expression of the structural similarity index becomes:

$$\mathrm{SSIM}(x,y) = \frac{(2\mu_x\mu_y + C_1)(2\sigma_{xy} + C_2)}{(\mu_x^2 + \mu_y^2 + C_1)(\sigma_x^2\sigma_y^2 + C_2)}\,. \tag{10}$$

Finally the quality measurement can provide a spatial map of the local image quality, which provides more information on the image quality degradation, which is useful in medical imaging applications.

For application, we require a single overall measurement of the whole image quality that is given by the following formula:

$$\mathrm{MSSIM}(I,\hat{I}) = \frac{1}{M}\sum_{i=1}^{M}\mathrm{SSIM}(I_i,\hat{I}_i), \tag{11}$$

where I and $\hat{I}$ are respectively the reference and degraded images, I_i and $\hat{I}_i$ are the contents of images at the i-th local window.

M is the total number of local windows in image. The MSSIM values exhibit greater consistency with the visual quality.

6   Results and Discussion

We are interested in lossy compression methods based on 2D wavelet transforms because their properties are interesting. Indeed, the 2D wavelets transform combines good spatial and frequency locations. As we work on medical image, the spatial location and frequency are important [22, 23].

We applied the proposed algorithm on test image 'Lena' of size 512×512 encoded by 8bpp.

Fig. 7 – *Original image.*

The importance of our work lies in the possibility of reducing the rates for which the image quality remains acceptable. Estimates and judgments of the

compressed image quality is given by the PSNR evaluation parameters and the MSSIM similarity Index.

Fig. 8 shown below illustrates the compressed image quality for different bit-rate values (number of bits per pixel).

To show the performance of the proposed method, we will now make a comparison between these different types of transform (CDF 9/7 (Filter Bank); Gall5/3 (Lifting scheme) and CDF9/7 (Lifting scheme)) coupled with the SPIHT coding and CDF9/7 (Lifting scheme) combined with the EZW coding. For each application we vary the bit-rate 0.125 to 2, and we calculate the PSNR and MSSIM. The results obtained are given in **Table 2**.

| (a) Ratio = 98.44 % ; PSNR = 24.50dB MSSIM = 0.68 | (b) Ratio = 96.88 % ; PSNR = 30.60 dB MSSIM = 0.84 | (c) Ratio = 93.75% ; PSNR = 35.41 dB MSSIM = 0.91 |
| (d) Ratio = 90.63%; PSNR = 37.74 dB MSSIM = 0.93 | (e) Ratio = 87.50 %; PSNR = 39.36 dB MSSIM = 0.95 | (f) Ratio = 75.00%; SNR = 43.88 dB MSSIM = 0.98 |

Fig. 8 – *Lena image compressed with* CDF9/7 (*Lifting scheme*) *and* SPIHT *coding.*

Table 2
PSNR *and* MSSIM *variation using different methods* (*Lena*).

R_c (bpp)	CDF9/7 (Lifting) + SPIHT		Gall5/3 (Lifting) + SPIHT		CDF9/7(Filter bank) + SPIHT		CDF9/7 (Lifting) + EZW	
	PSNR	MSSIM	PSNR	MSSIM	PSNR	MSSIM	PSNR	MSSIM
0.125	24.50	0.68	25.41	0.71	23.55	0.67	23.37	0.64
0.25	30.60	0.84	30.56	0.84	27.97	0.80	27.52	0.76
0.5	35.41	0.91	34.92	0.90	32.33	0.88	32.31	0.86
0.75	37.74	0.93	37.20	0.93	35.80	0.92	34.25	0.90
1	39.36	0.95	38.78	0.94	36.63	0.93	35.97	0.91
1.5	41.61	0.96	41.25	0.96	38.66	0.95	38.40	0.94
2	43.88	0.98	43.24	0.97	41.37	0.97	39.65	0.95

In this article we have applied our algorithm to compress medical images. For this reason, we have chosen an axial slice of human brain size 512x512 (grayscale) encoded on 8 bits per pixel, recorded by means of an MRI scanner (Fig. 9). This image is taken from the GE Medical System database [24].

Fig. 9 – *Original image* (*Brain Axial slice*).

Fig. 10 illustrates the compressed image quality for different bit-rate values (number of bits per pixel). According to the PSNR and MSSIM values, we note that from 0.5bpp, image reconstruction becomes almost perfect.

To show the performance of the proposed method, we make a comparison between these different types of transform (CDF 9/7 (Filter Bank); Gall5/3 (Lifting scheme) and CDF9/7 (Lifting scheme)) coupled with the SPIHT coding and CDF9/7 (Lifting scheme), combined with the EZW coding. For each application we vary the bit-rate from 0.125 to 2, and we calculate the PSNR and MSSIM. The results obtained are given in **Table 3**.
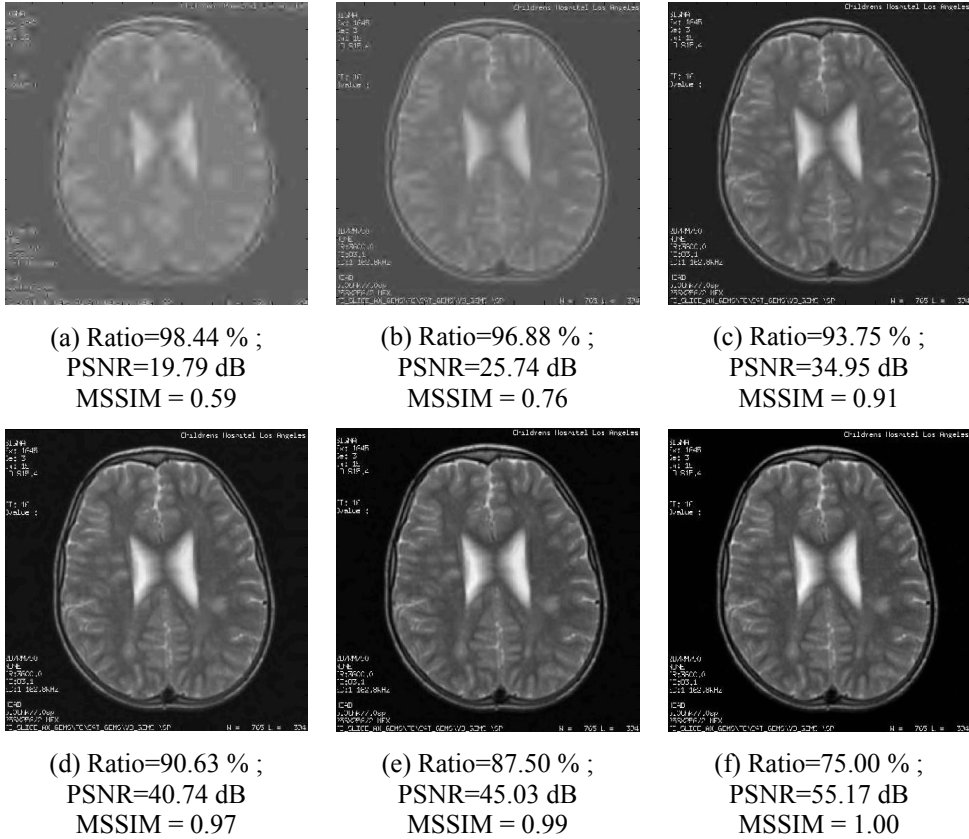
(a) Ratio=98.44 % ;
PSNR=19.79 dB
MSSIM = 0.59

(b) Ratio=96.88 % ;
PSNR=25.74 dB
MSSIM = 0.76

(c) Ratio=93.75 % ;
PSNR=34.95 dB
MSSIM = 0.91

(d) Ratio=90.63 % ;
PSNR=40.74 dB
MSSIM = 0.97

(e) Ratio=87.50 % ;
PSNR=45.03 dB
MSSIM = 0.99

(f) Ratio=75.00 % ;
PSNR=55.17 dB
MSSIM = 1.00

Fig. 10 – *Compressing of a axial slice with* CDF9/7
(*Lifting scheme*) *and* SPIHT *coding.*

The comparison in terms of image quality for the four algorithms is given by the PSNR and MSSIM curves represented in Figs. 11 and 12.

By comparing the different values of PSNR and MSSIM, we show clearly the effectiveness of our algorithm in terms of compressed image quality.

This study was subsequently generalized to a set of medical images of the GE Medical Systems database. The Fig. 13 presents the results obtained after application of our algorithm on various slices. These results are obtained with a 0.75 bpp bite-rate. We note that our algorithm is adapted for the MRI medical image compression.

We can observe that compression degrades to a lessen extent the image structure for a low compression bit-rate. However, for high compression bit-rate, our algorithm better safeguards the various image structures.

Table 3
PSNR *and* MSSIM *variation using different methods* (*Axial slice*).

| R_c (bpp)	CDF9/7 (Lifting) + SPIHT		Gall5/3 (Lifting) + SPIHT		CDF9/7 (Filter bank) + SPIHT		CDF9/7 (Lifting) + EZW	
	PSNR	MSSIM	PSNR	MSSIM	PSNR	MSSIM	PSNR	MSSIM
0.125	19.79	0.59	19.46	0.65	18.38	0.59	19.44	0.58
0.25	25.74	0.76	24.93	0.77	23.62	0.63	22.65	0.70
0.5	34.95	0.91	34.14	0.91	32.22	0.80	29.85	0.82
0.75	40.74	0.97	40.21	0.97	37.88	0.89	34.61	0.90
1	45.03	0.99	44.38	0.99	42.32	0.95	37.93	0.94
1.5	50.76	1.00	50.04	1.00	48.07	0.98	43.27	0.98
2	55.17	1.00	54.35	1.00	52.19	0.99	46.77	0.99
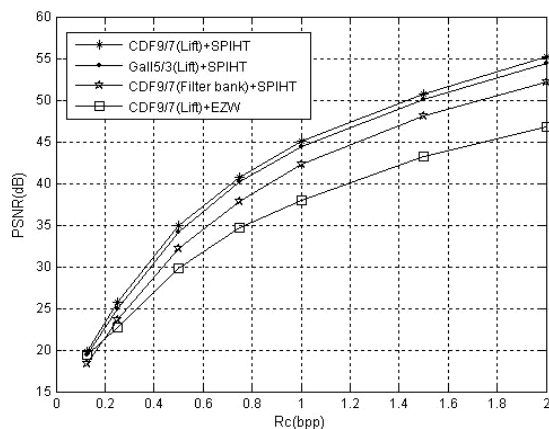
Fig. 11 – PSNR *variation using different methods*.
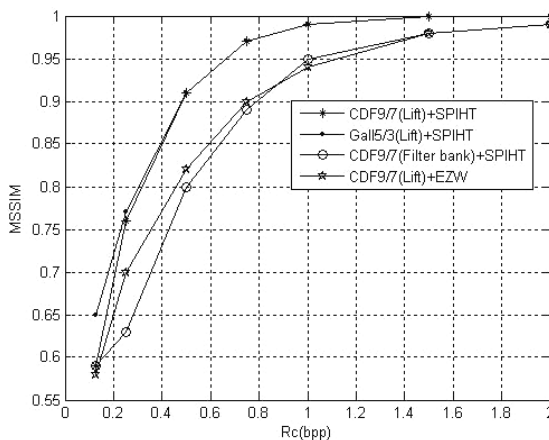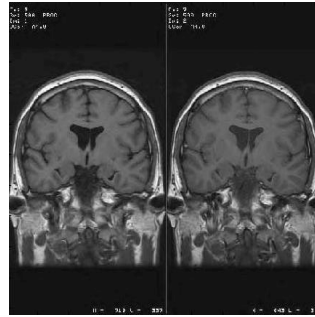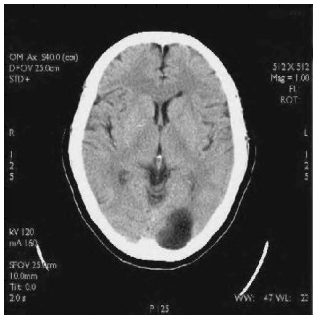

Fig. 12 – MSSIM *variation using different methods*.

Axial Slice of the brain (MRI)
Ratio = 90.63 % ;
PSNR = 39. 49 dB
MSSIM = 0.96

Coronal Slice of the brain (MRI)
Ratio = 90.63 % ;
PSNR = 36.45dB
MSSIM = 0.94

Axial Slice of the brain (CT)
Ratio = 90.63 % ;
PSNR = 36.10 dB
MSSIM = 0. 92

Echography image
Ratio = 90.63 % ;
PSNR = 35.68 dB
MSSIM = 0. 92

Fig. 13 – *Compressing of different slices by* CDF9/7 (*Lifting scheme*) *and* SPIHT *coding.*

7   Conclusion

The objective of this paper is undoubtedly the enhancement of medical images quality after the compression step. The latter is regarded as an essential tool to aid diagnosis (storage or transmission) in medical imaging. We used the Biorthogonal CDF9/7 wavelet compression based on lifting scheme, coupled with the SPIHT coding. After several applications, we found that this algorithm gives better results than the other compression techniques.

To develop our algorithm, we have applied this technique on different types of medical images. We have noticed that for 0.75 bpp bit-rate, the algorithm provides very important PSNR and MSSIM values for MRI images and it is more suitable for this category of images. Thus, we conclude that the results

obtained are very satisfactory in terms of compression ratio and compressed image quality. In perspective, we aspire to apply our algorithm to compress video sequences.

8   References

[1]   V. Chappelier: Progressive Coding of Images by Directed Wavelet, Phd Thesis, Rennes 1 University, 2005.

[2]   S. Mallat: Multifrequency Channel Decompositions of Images and Wavelet Models, IEEE Transaction in Acoustic, Speech and Signal Processing, Vol. 37, No. 12, Dec. 1989, pp. 2091 – 2110.

[3]   Said, W.A. Pearlman: An Image Multiresolution Representation for Lossless and Lossy Compression, IEEE Transactions on Image Processing, Vol. 5, No. 9, Sept. 1996, pp. 1303 – 1310.

[4]   Zandi, J.D. Allen, E.L. Schwartz, M. Boliek: CREW: Compression with Reversible Embedded Wavelets, Data Compression Conference, Snowbird, USA, March 1995, pp. 212 – 221.

[5]   A.R Calderbank, I. Daubechies, W. Sweldens, B.L. Yeo: Wavelet Transforms that Map Integers to Integers, Applied and Computational Harmonic Analysis, Vol. 5, No. 3, July 1998, pp. 332 – 369.

[6]   W. Sweldens. The Lifting Scheme: A Custom-design Construction of Biorthogonal Wavelets. Applied and Computational Harmonic Analysis, Vol. 3, No. 2, April 1996, pp. 186 – 200.

[7]   S.G. Miaou, S.T. Chen, S.N. Chao: Wavelet-based Lossy-to-lossless Medical Image Compression using Dynamic VQ and SPIHT Coding, Biomedical Engineering: Applications, Basis & Communications, Vol. 15, No. 6, Dec. 2003, pp. 235 – 242.

[8]   M. Antonini, M. Barlaud, P. Mathieu, I. Daubechies: Image Coding using Wavelet Transform, IEEE Transactions on Image Processing, Vol. 1, No. 2, April 1992, pp. 205 – 220.

[9]   Said, W.A. Pearlman: A New, Fast and Efficient Image Codec based on Set Partitioning in Hierarchical Trees, IEEE Transaction on Circuits and Systems for Video Technology, Vol. 6, No. 3, June 1996, pp. 243 – 250.

[10]   J.D. Villasenor, B. Belzer, J. Liao: Wavelet Filter Evaluation for Image Compression, IEEE Transactions on Image Processing, Vol. 4, No. 8, Aug. 1995, pp.1053 – 1060.

[11]   D.S. Taubman, M.W. Marcellin: JPEG2000: Image Compression Fundamentals, Standards and Practice, Kluwer Academic Publishers, London, 2002.

[12]   G. Pau: Advanced Wavelets and Space-time Decompositions: Application to Video Coding Scalable, Phd thesis, National School of Telecommunications, Paris, 2006.

[13]   Savakis, R. Carbone: Discrete Wavelet Transform Core for Image Processing Applications, Real-time Imaging IX, SPIE-IS&T Electronic Imaging, San Jose, CA, USA, SPIE Vol. 5671, Jan. 2005, pp. 142 – 151.

[14]   Daubechies, W. Sweldens: Factoring Wavelet Transforms into Lifting Steps, Journal of Fourier Analysis and Applications, Vol.4, No. 3, May 1998, pp. 247 – 269.

[15]   P.S.A. Kumar: Implementation of Image Compression Algorithm using Verilog with Area, Power and Timing Constraints, Master Thesis, National Institute of Technology, Rourkela, India, 2009.

[16] Y.Y. Chen, S.C. Tai: Embedded Medical Image Compression using DCT based Subband Decomposition and Modified SPIHT Data Organization, IEEE Symposium on Bioinformatics and Bioengineering, Taichung, Taiwan, May 2004, pp. 167 – 175.

[17] Z. Xiong, K. Ramchandran, M.T. Orchard: Space-frequency Quantization for Wavelet Image Coding, IEEE Transaction on Image Processing, Vol. 6, No. 5, May 1997, pp. 677 – 693.

[18] W.S. Geisler, M.S. Banks: Visual Performance, Handbook of Optics – Vol. 1, McGraw-Hill, NY, USA, 1995.

[19] A.B. Watson, L.B. Kreslake: Measurement of Visual Impairment Scales for Digital Video, Human Vision and Electronic Imaging Conference, San Jose, CA, USA, SPIE Vol. 4299, Jan. 2001, 2001, pp. 79 – 89.

[20] Z. Wang, A.C. Bovik., H.R. Sheikh, E.P. Simoncelli: Image Quality Assessment: From Error Visibility to Structural Similarity, IEEE Transactions on Image Processing, Vol. 13, No. 4, April 2004, pp. 600 – 612.

[21] Z. Wang, A.C. Bovik: A Universal Image Quality Index, IEEE Signal Processing Letters, Vol. 9, No. 3, March 2002, pp. 81 – 84.

[22] R.W. Buccigrossi, E.P. Simoncelli: Image Compression via Joint Statistical Characterization in the Wavelet Domain, IEEE Transaction on Image Processing, Vol. 8, No. 12, Dec. 1999, pp. 1688 – 1701.

[23] D.M. Chandler, S.S. Hemami: Additivity Models for Suprathreshold Distortion in Quantized Wavelet-coded Images, Human Vision and Electronic Imaging Conference, San Jose, CA, USA, SPIE Vol. 4662, May 2002, pp. 105 – 118.

[24] www.gehealthcare.com.

[25] A.M. Lakhdar, R. Méliani, M. Kandouci: Robust Image Transmission Performed by SPIHT and Turbo-codes, Serbian Journal of Electrical Engineering Vol. 5, No. 2, Nov. 2008, pp. 353 – 360.

[26] K. Kannan, S.A. Perumal, K. Arulmozhi: Optimal Decomposition Level of Discrete, Stationary and Dual Tree Complex Wavelet Transform for Pixel based Fusion of Multi-focused Images, Serbian Journal of Electrical Engineering Vol. 7, No. 1, May 2010, pp. 81 – 93.